UDC666.7:666.3. 046.4

# Firing of Large-Sized Engineering Ceramic Parts

Shoichi Harato*1
Junzo Hasegawa*1
Hiromi Matsumoto*3
Mitsuo Sugawara*2
Tatsuro Mitsudome*2
Yoshiaki Hara*1
Tetsuro Nose*3

**Abstract:**

*Nippon Steel has developed a stable firing technology for large-sized engineering ceramic parts for structural use on which its New Materials Divisions Group has researched for commercialization. The development work consisted of four parts: investigation of dewaxing process, investigation of sintering process, measurement of actual heat transfer in the furnace during firing, and computer simulation of the firing process. The findings and techniques obtained have made it possible to stably produce large-sized engineering ceramic parts that were difficult to fire by the conventional empirical methods.*

## 1. Introduction

Nippon Steel Corporation and KROSAKI Corporation carried out the joint development of advanced structural engineering ceramics from October 1985 to October 1989, and have established manufacturing conditions for simple and small parts (plates, columns, and cylinders) of alumina, zirconia, sialon, and silicon carbide.

During the period of development, however, the target products increased in both size and complexity, to the extent that a mere extension of techniques based on empirical knowledge could not establish crack- and defect-free ceramic firing conditions, which seriously inhibited the progress of development. The situation indicated the necessity of more accurately understanding the firing process, and optimizing the sintering conditions with a view to low cost, stable quality and short delivery lead time.

Against the above background, the authors undertook the development of stable firing technology for large-sized ceramic parts with the following objects:

(1) Quantification of phenomena occurring in each stage of firing
(2) Estimation of temperature and stress distributions during firing by computer simulation
(3) Optimization of firing conditions

This report describes the approaches adopted to the technology, development, results obtained for each stage of firing process, and examples of their actual application results.

## 2. Description of Development Project

### 2.1 Development approaches

The approaches adopted to the development of firing technology are conceptually illustrated in **Fig. 1**. The firing process generally involves setting green compacts in the furnace, and heating, cooling and consolidating the compacts by controlling the furnace atmosphere temperature. It consists of four main stages: dewaxing, heating, sintering, and cooling.

The present firing process is premised on heat transfer from the surfaces of green compacts. Changing the atmosphere temperature inevitably creates a temperature distribution in the compact. In addition, stresses are induced in the compact by the thermal decomposition gas generated in the dewaxing stage, by nonuniform shrinkage in the sintering stage, and by the temperature distribution in the heating and cooling stages. To obtain a sound fired body, the firing must be completed while controlling the stress generation in each stage under the strength of the green compact.

The present development work followed the course of quan-

*1 New Materials Divisions Group
*2 KROSAKI Corporation
*3 Technical Development Bureau

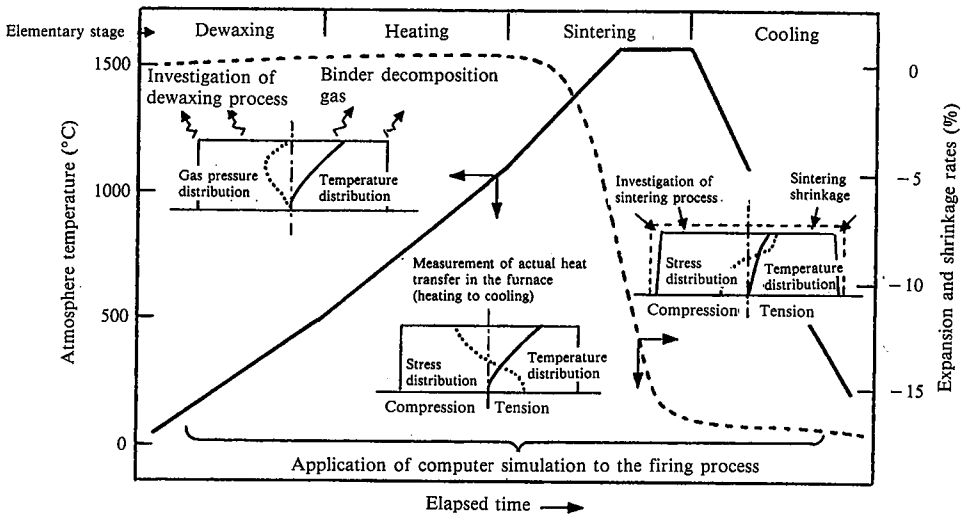


**Fig. 1** Conceptual illustration of development approaches

tifying the heat transfer, dewaxing and sintering phenomena during firing; estimating temperature and stress variations in the compact by simulating the entire firing process; and establishing optimum firing conditions.

The ceramic part selected as the object of development is a large part for X-Y stage of alumina containing zirconia (tetragonal zirconia), as shown in **Photo 1**.

### 2.2 Investigation of dewaxing phenomena

To determine factors responsible for cracking during the dewaxing stage where organic binders are removed by heating, the thermal decomposition behavior of binders and the weight loss and dimensional changes of compacts during heating were investigated, while the rise of gas pressure in the compact through thermal decomposition were estimated. The following findings therefrom were obtained:

(1) As shown in **Fig. 2**, it was confirmed that the binder (polyvinyl alcohol system) is thermally decomposed with temperature rise, that the thermal decomposition progresses to 60 and 70% at around 300°C in both the air stream and nitrogen steam, and to about 95% at 700°C even in the nonoxidizing atmosphere. From the combined results of measurements of thermogravimetry (TG) and mass spectrometry (MS) the thermal decomposition products of the binder in the inert atmosphere was identified mainly as carbon monoxide, carbon dioxide, water vapor, and acetaldehyde, as shown in **Fig. 3**.

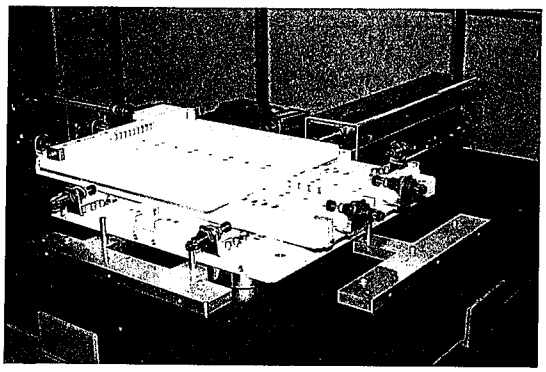

**Photo 1** Large-sized ceramic part for X-Y stage
Material: Zirconia-containing alumina
Dimensions: 510 mm × 500 mm × 43 mm

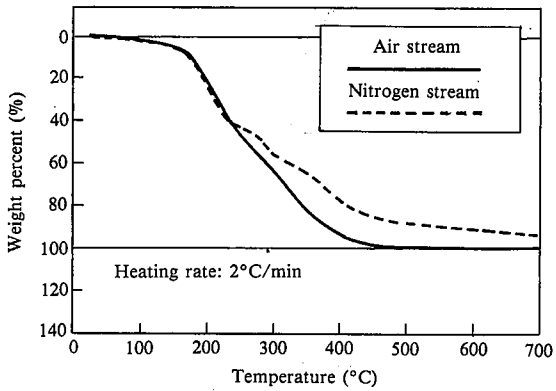


**Fig. 2** Thermal decomposition curve for binder (in air stream and nitrogen stream)

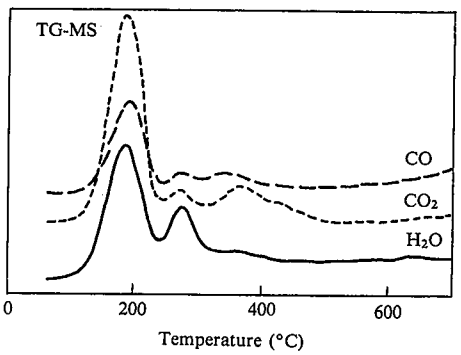


**Fig. 3** Individual ion intensity during thermal decomposition of binder

(2) Investigation of the weight loss and dimensional change of compacts revealed that zirconia-containing alumina increases in size with dewaxing, but abnormally turns from expansion to shrinkage at 250°C, as shown in **Fig. 4**. It was comfirmed that the phase transformation of zirconia from tetragonal phase to monoclinic was involved in this expansion and abnormal shrinkage.

(3) The pressure rise in the green compact due to the thermal

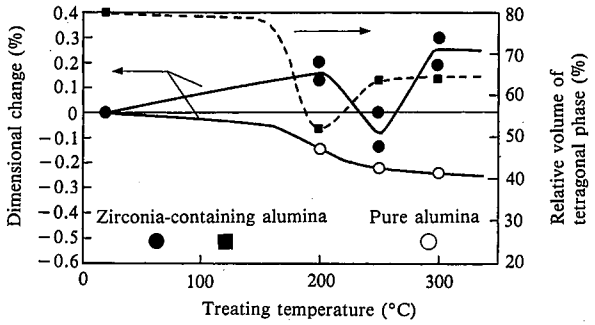


**Fig. 4** Dimensional change and variation of relative valume of tetragonal phase in zirconia due to heating

decomposition gas was estimated on the basis of the measured values of binder decomposition rate and compact permeability.

Isothermal gravimetric analysis found that the decomposition rate up to about 250°C could be expressed as first-order reaction by Eq. (1) and that the activation energy for the decomposition was 158kJ/mol.

$$\xi = 1 - \exp(-k_0 t) \quad \cdots\cdots(1)$$

where $\xi$ is decomposition rate; t is holding time; and $k_0$ is reaction rate constant ($2.78 \times 10^{-5}$/s).

Gas permeability measurements indicated that the relationship between the amount of dewaxing and the permeability can be explained well by Eq. (2), the Kozeny-Carman equation.

$$a = \frac{\varepsilon^3}{45(1-\varepsilon)^2} r_p^2 \quad \cdots\cdots(2)$$

where a is permeability; $\varepsilon$ is porosity; and $r_p$ is mean pore radius.

One-dimensional unsteady-state simulation was performed with regard to the gas pressure generated at the center of the compact, as shown in **Fig. 5**, using Eqs. (1) and (2) together with the thermal conductivity and the specific heat data of the compacts, and assuming that the gas transfer follows the diffusion equations. **Fig. 5** shows that the maximum gas pressure at the center of the compact is approximately proportional to the compact thickness and that the pressure increases by 30% when the holding temperature is raised by about 20°C. The relationship among the maximum gas pressure, heating rate, compact thickness, and permeability under isokinetic heating conditions is given by

$$P_{max} = \frac{K\left(\frac{dT}{dt}\right)^{0.5} \cdot d}{a^{0.5}} \quad \cdots\cdots(3)$$

where $P_{max}$ is the maximum internal gas pressure; K is constant; $dT/dt$ is heating rate; and d is compact thickness.

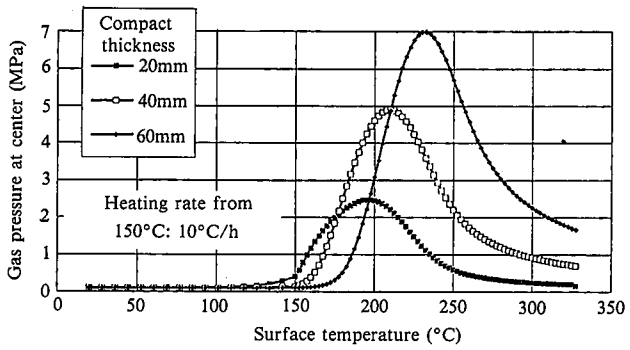


**Fig. 5** Example of simulation of gas pressure at center of compacts

The above discussion emphasizes the need for strict temperature control in order to prevent the cracking of the green compacts due to the thermal decomposition gas in the dewaxing stage of large ceramic parts.

### 2.3 Investigation of sintering phenomena

2.3.1 Thermal and kinetic investigation of sintering process[1, 2]

The constant rate heating and isothermal shrinkage behavior of zirconia-containing alumina was investigated by dilatometry. An attempt was also made to formulate the sintering shrinkage of ceramics using isothermal shrinkage data.

(1) **Fig. 6** shows the results of shrinkage measurement made of zirconia-containing alumina during constant rate heating at 0.5, 1, 2, and 4°C/min, respectively. Sintering started at about 1,200°C, and the shrinkage at the maximum test temperature of 1,500°C was 13.4, 12.5, 11.7 and 9.5% at the heating rates of 0.5, 1, 2 and 4°C/min, respectively. The shrinkage rate reached its maximum ($7 \times 10^{-4}$/°C) at each heating rate when the shrinkage was about 9%, and declined with increasing shrinkage. The temperature at which the shrinkage rate became the maximum was 1,410, 1,440, 1,460, and 1,490°C at the heating rates of 0.5, 1, 2, and 4°C/min, respectively.

Another experiment found that when a compact was heated to 1,575°C, it shrunk by 17.1%, a value close to the calculated shrinkage of 17.3%, and was fully densified.

(2) The isothermal shrinkage measurement results are shown in **Fig. 7**. The diffusion-controlled shrinkage of a single-phase powder system composed of ideal spherical particles in the initial stage of sintering during isothermal heating is expressed by Eq. (4), where the proportionality constant q is 0.33 to 0.4. The value of q calculated from actual measurement data was found to

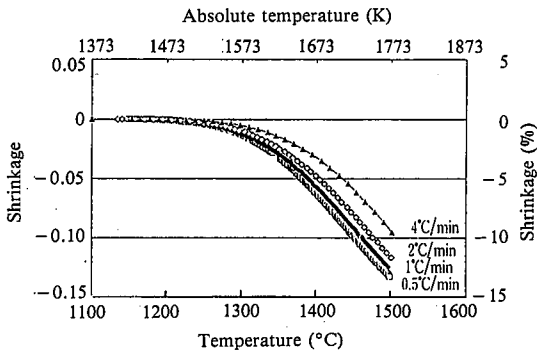


**Fig. 6** Shrinkage curves under constant-rate heating

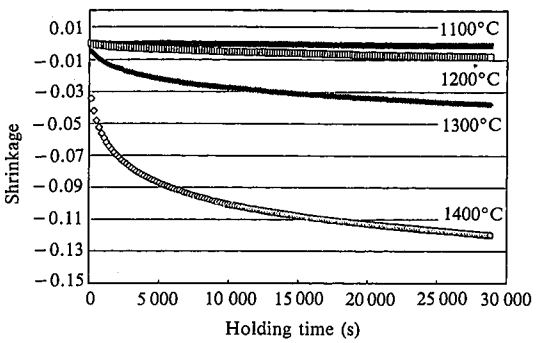


**Fig. 7** Isothermal shrinkage curves

monotonically decrease with the progress of sintering.

$$\ln(f) = q \cdot \ln\left(\frac{KDt}{kT_k r^p}\right) \quad \cdots\cdots(4)$$

where f is shrinkage; $T_k$ is absolute temperature; t is elapsed time; r is particle radius; D is diffusion coefficient in controlling factor for diffusion mechanism; k is Boltzmann constant; p and q are constants governed by the diffusion mechanism.

(3) Eq. (4) is a theoretical equation applicable to the initial stage of sintering when shrinkage is small, but may be applied to the entire shrinkage range of interest if q is considered as its variable. Analysis of isothermal shrinkage data confirmed that q can be regressed by the primary function of ln(f) at each temperature.

$$q = d\ln(f)/d\ln(t) = C_1 \cdot \ln(f) + C_2$$

Using the regression coefficients $C_1$ and $C_2$, the relationship between the shrinkage and the elapsed time at any desired temperature was formulated as:

$$\ln(f) = (1/C_1)(S \cdot t^{C_1} - C_2) \quad \cdots\cdots(5)$$

Comparison of Eq. (4) with an equation differentiated by the logarithm of time yields the following equations:

$$\left.\begin{aligned} C_1 &= d\ln(q)/d\ln(t) \\ C_2 &= q\{1 - d(p \cdot \ln(r))/d\ln(t)\} \\ S &= q/t^{C_1} \end{aligned}\right\} \quad \cdots\cdots(6)$$

The parameters $C_1$, $C_2$, and S are all formulated as a function of temperature. $C_1$ and S indicate that the sintering mechanism is not constant but changes from time to time. $C_2$ is considered to be related to microstructural evolution as represented by the particle size.

(4) When the microstructural change of green compacts in the sintering process was observed in detail, it was confirmed that grains of nanometer size first disappeared with the progress of sintering and that the average grain size then gradually increased.

From the above results, it was estimated that the sintering of zirconia-containing alumina proceeds in the temperature range of about 1,200 to 1,575°C. Since the shrinkage rate is the highest from 1,400 to 1,500°C, the compacts should be heated most moderately through this temperature region when cracking due to the difference of sintering shrinkage rate becomes a problem.

2.3.2 Investigation of high-temperature plastic deformation during sintering[3,4]

Even, ceramics exhibit plasticity at elevated temperatures. To estimate the stresses generated in the ceramic compact during sintering and cooling, the relationship between stress and strain in high-temperature plasticity must be clarified. Using a bending test machine, the stress-strain relations in high-temperature plasticity were measured for fully sintered bodies (in the cooling stage) and partially sintered compacts (in the sintering stage), adopting a constant strain rate.

(1) As shown in **Fig. 8**, the fully sintered bodies exhibited plastic deformation at 1,360°C and above. It was confirmed that the stress first increases monotonically and then stabilizes in the steady state (this stress to be hereinafter called the flow stress). The logarithmic values of the flow stress and the strain rate are linearly related as shown in **Fig. 9**, and the slope (hereinafter called the stress exponent) of the linear relation is approximately unity. It was found that the higher the temperature, the lower the flow stress. The apparent activation energy for high temperature deformation could also be estimated from Arrhenius plots.

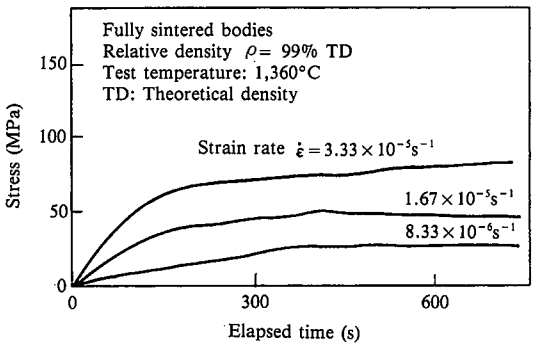


**Fig. 8** High-temperature plasticity of fully sintered bodies

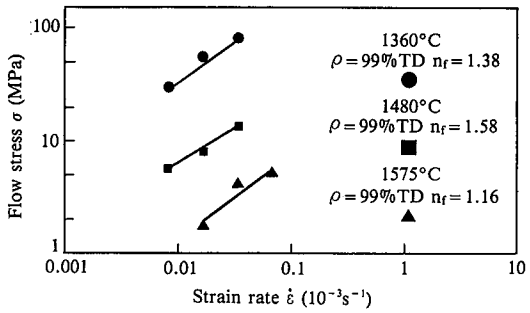


**Fig. 9** Flow stress versus strain rate of fully sintered bodies

The above results indicated that the high-temperature plasticity of fully sintered bodies occurs through a diffusion. The relationship among the flow stress, temperature, and strain rate was thus formulated as given by:

$$\dot{\varepsilon} = K_f \sigma^{n_f} \exp\left(-\frac{Q_f}{RT_k}\right) \quad \cdots\cdots(7)$$

where $\dot{\varepsilon}$ is strain rate; $\sigma$ is flow stress; $Q_f$ is apparent activation energy for the deformation (473 kJ/mol); R is gas constant; $n_f$ is stress exponent (1.37); and $K_f$ is constant.

(2) Few studies are available on the high-temperature plastic behavior of partially sintered compacts. Using compacts partially sintered at arbitrary temperature levels, stress variation was investigated under the same temperature as the partial sintering temperature. The partially sintered compacts exhibited plastic behavior in the temperature region of 1,100°C and above. As in the fully sintered bodies, stress was found to monotonically increase and then progress at a constant value. The logarithmic values of the flow stress and strain rate are linearly related as shown in **Fig. 10**. Unlike the fully sintered bodies, however, the stress level was found to decrease first with increasing temperature and then to shift to an increase, and the stress exponent was found to decline from about 3 to about 2 and then again increase.

This was attributed to a change in the mechanism of plasticity with the progress of sintering, as exemplified by the decrease in the porosity and increase in the density of the partially sintered compacts with increasing temperature, and further by the increase in the size of ceramic particles with grain growth. From the above findings, the following empirical equation was derived, allowing for the effects of density (porosity) and grain size as well as temperature:

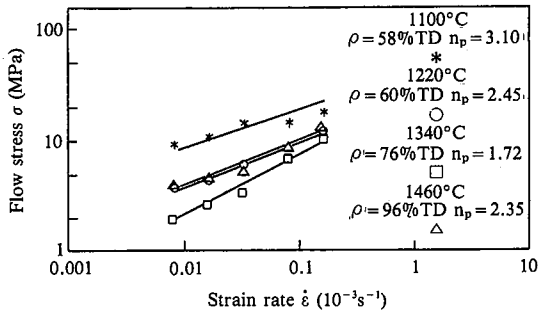


**Fig. 10** Flow stress versus strain rate of partially sintered compacts

$$\dot{\varepsilon} = K_p \frac{\sigma^{n_p}}{T_k d_0^m \rho^l} \exp\left(-\frac{Q_p}{RT_k}\right) \quad \cdots\cdots(8)$$

where $Q_p$ is apparent activation energy; $d_0$ is normalized grain size; $\rho$ is relative density; $K_p$ is constant; $n_p$ is stress exponent (function of temperature); m is exponent for the effect of grain size; and l is exponent for the effect of density.

### 2.4 Measurements of heat transfer in firing furnace

To quantify the heat transfer mechanism in the firing furnace and particularly inside the green compacts, temperature measurement was made of a green compact prepared in the shape of a flat plate resembling an actual large ceramic part, using a small electric furnace and thermocouples. This was to clarify the temperature distribution and its transition in the green compact under various firing schedules and conditions. The effect of the size (thickness and width) of the green compact was also examined.

**Figs. 11** and **12** show examples of temperature measurement made. **Fig. 11** shows the atmosphere temperature and the temperature difference between the top and bottom surfaces of the green compact under a small-shape firing pattern, with and without a muffle used in the furnace. **Fig. 12** shows differences in the temperature distribution of the compact at the atmosphere temperature of 800°C when the compact was fired under different patterns. These temperature measurements resulted in the following clarification:

(1) As shown in **Figs. 11** and **12**, the widest temperature difference occurs in the heating stage from the end of dewaxing to the start of sintering. The temperature difference develops in approximate proportion to the heating rate. This is due to the low thermal conductivity of the dewaxed materials and partially sintered compacts. It was also found that cracking occurs when temperature difference reaches about 200°C over the compact thickness range of 40 mm.

(2) As shown in **Fig. 11**, it was found that the temperature difference in the compact rapidly decreases with the progress of densification in the sintering stage. This is probably because the rise of density with the progress of sintering rapidly improves the ther-

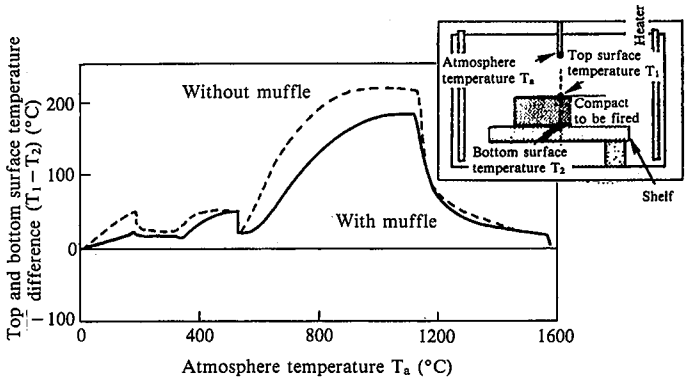


**Fig. 11** Examples of measurements of temperature distribution and temperature change with regard to partially sintered compacts

| Pattern | Heating rate in medium-temperature region (°C/h) | Top and bottom surface temperature difference (°C) | Cracking |
|---|---|---|---|
| Small shape pattern | 200 | 220 | Yes |
| Small shape + muffle | 200 | 196 | Yes |
| Small shape + hold | 200 | 184 | No |
| Medium shape pattern | 100 | 134 | No |
| Large shape pattern | 50 | 78 | No |

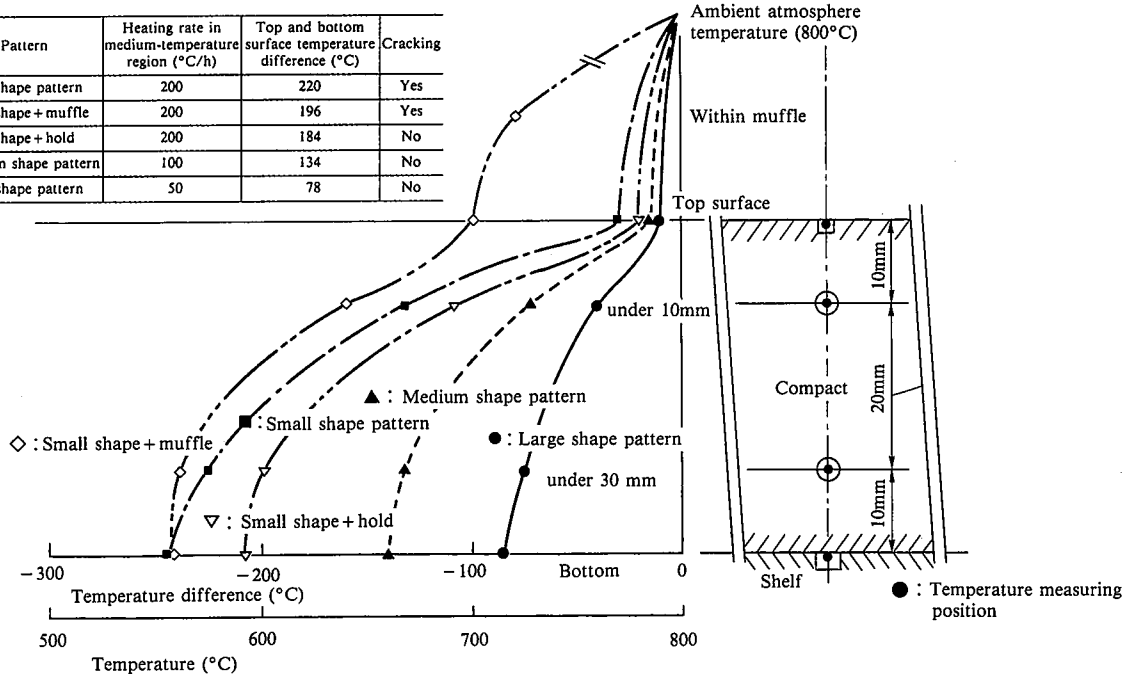


**Fig. 12** Temperature distributions in green compacts

mal conductivity of the compact. These results suggest that the heating rate should be held as low as possible, although it has been traditionally made generally higher than in the sintering stage.

(3) As shown in **Fig. 12**, various measures taken for temperature homogenization during firing, such as using a muffle or refractory envelop for the compacts and keeping the compacts at a constant temperature before entry into the dangerous temperature region, proved actually effective in equalizing the temperature distribution in the compacts.

### 2.5 Estimation of stress generation during firing by computer simulation

#### 2.5.1 Physical properties of compacts and boundary conditions for simulation[5]

In the firing process, the ceramic part changes in density as well as in thermal and mechanical properties with increasing temperature through the stage of precursor, dewaxed compact, partially sintered compact, and fully sintered body. These properties must be each formulated eventually as a function of temperature. Computer simulation of the firing process requires three equations, namely, sintering rate equation, equation for estimating the stress generated throughout the firing process, and equation for indicating the dependence of thermal properties on temperature and density.

(1) The sintering rate equation must be capable of describing the relationship between the density and temperature of the compact over the sintering stage from the start to the end of sintering. An attempt was made to formulate the sintering rate for the computer simulation of the firing process in parallel with the investigation of the sintering phenomena previously described. The sintering rate was successfully formulated for each level of heating rate by analyzing the ultimate temperature and density, using small disk samples and a small electric oven for measurement, as given by

$$d\rho/dt = (1-\rho)S_0\exp(S_1T+S_2T^2) \quad \cdots\cdots(9)$$

where t is time; T is temperature; and $S_0$, $S_1$, $S_2$ are regression constants.

(2) The stress estimation equation was formulated by measuring Young's modulus by the ultrasonic method and the compression method, and taking the density dependence of Young's modulus into account. On the basis of the results presented in the section concerning the high-temperature plasticity of compacts during sintering, a stress-strain constitutive equation capable of describing the high-temperature plasticity of the fully sintered body in the cooling stage and of the partially sintered compact in the sintering stage, both in the high-temperature plastic region, was formulated as follows:

$$\sigma = \sigma_0\exp\{-(Y_1T+Y_2T^2)\}\cdot\dot{\varepsilon}^{Y_3}\cdot\rho^{Y_4} \quad \cdots\cdots(10)$$

where $\sigma_0$, $Y_1$, $Y_2$, $Y_3$ are regression constants; and $Y_4$ is exponent indicating the effect of density. Taking into consideration the thickness of the green compact, a vertical constraint condition for the interface between the green compact and column plate as shown in **Fig. 13** was applied as a mechanical boundary condition.

(3) The temperature and density dependence of thermal properties was formulated by measuring the thermal conductivity of the compact by the laser flash method and the hot wire method and also taking into account the measurement results. The heat transfer coefficient and emissivity, which are thermal boundary conditions, were modified to suit the actual state of heat transfer in the firing furnace, thereby providing for the accuracy of firing simulation.

#### 2.5.2 Simulation of firing[5]

The firing process was simulated using an elastic-plastic FEM for compressible materials allowing large increment deformation[5] developed by the Mechanical Working Process Laboratory at Nippon Steel's Process Technology Research Laboratories. A disk, a perforated disk, and a cylinder were studied as model shapes. The results of calculation for the disk of a simple shape will be discussed here which can be readily correlated with the investigation of the actual heat transfer in the firing furnace as shown in **Fig. 13**.

The firing process was divided into three stages, that is, heating, sintering and cooling, for the purpose of simulation. **Fig. 14** shows some calculation results with the disk model. The simulation work made it possible to quantitatively estimate the temperature and stress changes and resultant distribution of compacts throughout the firing process and the shrinkage of compacts during sintering, and resulted in the following findings about the stress generated in the firing process:

(1) Heating stage: The largest temperature difference develops in the heating stage, and the thermal stress that is roughly proportional to the temperature difference is produced at the bottom surface of the disk compact. This heating stage is where the strength of the compact drops to minimum, resulting in the highest possibility of cracking. This points to the need for revising the conventional idea that the compact can be heated rather rapidly without any problem in the heating region for sintering after dewaxing.

(2) Sintering stage: Tensile stress is generated on the top surface of the compact in the early step of sintering, and on the bottom

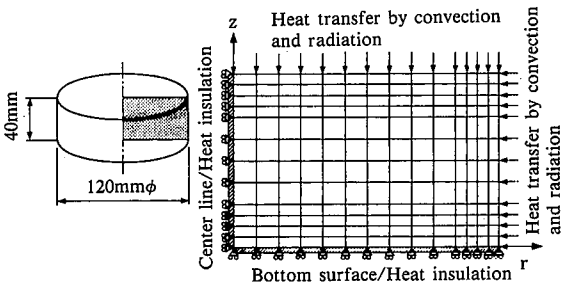


**Fig. 13** Schematic of disk model (120 mm diameter × 40 mm thick)

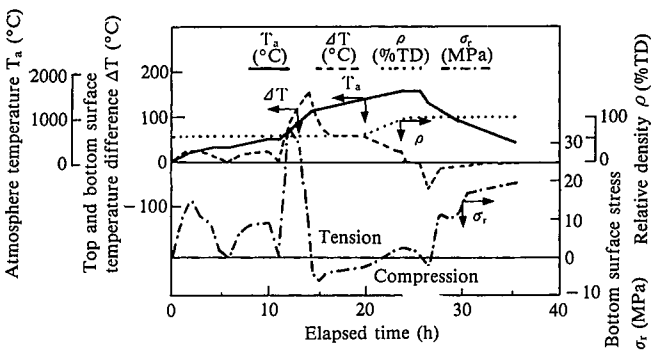


**Fig. 14** Example of firing simulation for disk model

surface of the compact in the last step of the sintering stage. The resultant stress is relaxed by the plasticity of the compact and is smaller in the absolute value than the one observed in the heating stage. It was thus estimated that the risk of stress-induced cracking would be less in the sintering stage.

(3) Cooling stage: The tensile stress probably resulting from heterogeneous thermal shrinkage was calculated to be present on the bottom surface of the compact. This suggests that internal stress remains even after firing.

### 2.6 Application to large-sized ceramic parts

The above-mentioned findings were applied to the actual firing of large-sized ceramic parts with the following special considerations:

(1) Hold the compact at such a temperature that the dewaxing rate becomes maximum, and accomplish the uniform and reasonable dewaxing.

(2) Add a holding stage in the medium-temperature region from 500 to 1,000°C in the heating stage to control the generation of temperature difference and stress in the compact.

(3) Install a double muffle on the furnace roof to suppress the heat transfer from the top of the compact and to promote a uniform temperature distribution.

(4) Do not use a green setter of the same material as the compact for reducing the friction with the hearth plate, lest it should widen the temperature variation, which, from an overall point of view, runs counter to the purposes of reducing the stress generation.

**Photo 2** shows a large-sized alumina ceramic part before and after the implementation of corrective measures. These countermeasures resulted in the successful firing of a large alumina ceramic X-Y stage part measuring 510 mm × 500 mm × 43 mm, as shown in **Photo 1.** This material was difficult to fire by conventional methods that are based on empiricism.

The firing techniques established through the development work under discussion are being applied successfully to firing practices for large-sized ceramic parts for electronic device and semiconductor processing facilities, as well as for wear-resistant and heat-resistant applications.

## 3. Conclusions

The firing process was divided into several stages and the phenomena occurring in each stage were investigated and quantified according to theory. Application of computer simulation to the entire firing process facilitated the estimation of temperature and stress distributions and their progresses in the compacts being fired. These results prompted switchover from empiricism to theory in setting up the compact firing conditions, which culminated in the establishment of a general-purpose ceramics firing technology for stably firing large-sized ceramic parts.

An extension of the new general-purpose firing technology are being pushing forward by the authors along with the development of a "near-net shape firing technology" for the production of ceramic parts of a shape almost identical to the end product shape.

**References**

1) Mitsudome, T. et al.: Proc. of 4th Autumn Symp. The Ceramic Society of Japan, 1991, p. 159
2) Mitsudome, T. et al.: Proc. of 1991 Autumn Joint Research Meeting, The Ceramic Society of Japan and Kyushu Chapter, Technical Association of Refractories, Japan, 1991, p. 43
3) Harato, S. et al.: Proc. of 4th Autumn Symp. The Ceramic Society of Japan, 1991, p. 171
4) Harato, S. et al.: Proc. of 1991 Autumn Joint Research Meeting, The Ceramic Society of Japan and Kyushu Chapter, Technical Association of Refractories, Japan, 1991, p. 67
5) Matsumoto, H. et al.: Shinnittetsu Giho. (342), 3 (1991)
6) Kamisawa, J. et al.: Porous Material Handbook. ICP, 1988
7) Kondo, R.: Porous Materials. Gihodo, 1973
8) The Ceramic Society of Japan: Fine Ceramics Engineering Handbook. 1st ed. Gihodo, 1989
9) Hamano, K.: Fine Ceramics Handbook. 1st ed. Asakura Shoten, 1988

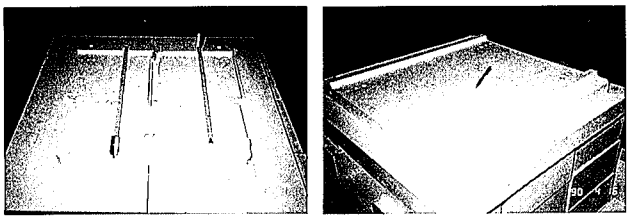

(a) Before implementation of corrective measures (b) After implementation of corrective measures (successful firing)

**Photo 2** Firing of large-sized alumina ceramic part before and after implementation of corrective measures